Available online at www.sciencedirect.com
ScienceDirect
Journal of Theoretical Biology 247 (2007) 525–543
Journal of Theoretical Biology
www.elsevier.com/locate/yjtbi

Coalescence of interacting cell populations

Matthew J. Simpson*, Kerry A. Landman, Kaushik Bhaganagarapu

Department of Mathematics and Statistics, University of Melbourne, Vic. 3010, Australia

Received 30 October 2006; received in revised form 27 February 2007; accepted 27 February 2007
Available online 14 March 2007

Abstract

We analyse the coalescence of invasive cell populations by studying both the temporal and steady behaviour of a system of coupled reaction–diffusion equations. This problem is relevant to recent experimental observations of the dynamics of opposingly directed invasion waves of cells. Two cell types, u and v, are considered with the cell motility governed by linear or nonlinear diffusion. The cells proliferate logistically so that the long-term total cell density, $u+v$ approaches a carrying capacity. The steady-state solutions for u and v are denoted u_s and v_s. The steady solutions are spatially invariant and satisfy $u_s+v_s=1$. However, this expression is underdetermined so the relative proportion of each cell type u_s and v_s cannot be determined *a priori*. Various properties of this model are studied, such as how the relative proportion of u_s and v_s depends on the relative motility and relative proliferation rates. The model is analysed using a combination of numerical simulations and a comparison principle. This investigation unearths some novel outcomes regarding the role of overcrowding and cell death in this type of cell migration assay. These observations have relevance to experimental design and interpretation regarding the identification and parameterisation of mechanisms involved in cell invasion.

Keywords: Cell invasion; Coalescence; Interacting populations; Diffusion; Proliferation; Cell death

1. Introduction

Mathematical models of cell migration have been traditionally developed to describe the dynamics of systems with one cell type (Keller and Segel, 1970; Murray, 2002). Although these models have successfully explained experimental observations (Maini et al., 2004a, 2004b; Savla et al., 2004) and provided deeper insight into biological phenomena (Savla et al., 2004; Tyson et al., 1999), it is likely that most practical modelling will depend on simulating the interactions of many cell types (Wolpert, 2002).

The use of multispecies modelling to represent cell migration phenomena has become standard in many applications. For example, multispecies modelling is used in both continuum and discrete frameworks to simulate cell migration in a variety of contexts including cell sorting (Merks and Glazier, 2005), embryonic morphogenesis (Longo et al., 2004), microvasculature patterning (Peirce et al., 2004), avascular tumour development (Perumpanani et al., 1997), and the development of the enteric nervous system (ENS) (Simpson et al., 2006b, 2007).

In this analysis we focus on cell invasion phenomena involving the interaction of two opposingly directed cell invasion waves. A schematic diagram of this process is given in Fig. 1 where two invasion waves are shown moving towards each other and simultaneously invading the unoccupied space between them. We are particularly interested in the dynamics of the system after the two invasion waves intersect and the details of how the two populations coalesce over long periods of time.

1.1. Previous work on interacting invasion models

The wound healing model developed and analysed by Sherratt (2000) proposed that contact inhibition of motility can be a dominant mechanism influencing systems with significant cell–cell contact. In this work the nonlinear cell diffusivity was written as a fraction of each cell type present. The movement of each cell type was assumed to be proportional to the macroscopic gradient of the total cell density (Witelski, 1997) rather than being proportional to

*Corresponding author. Tel.: +613 8344 6517; fax: +613 8344 4599.
E-mail address: m.simpson@ms.unimelb.edu.au (M.J. Simpson).

0022-5193/$ - see front matter © 2007 Elsevier Ltd. All rights reserved.
doi:10.1016/j.jtbi.2007.02.020

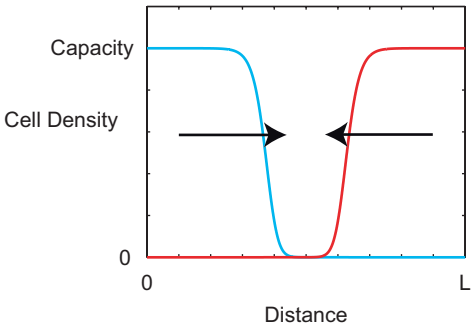

Fig. 1. Schematic diagram showing two invading cell populations advancing towards each other. The blue cell population is invading to the right while the red population is invading to the left. After some time the two populations intersect and coalesce.

the macroscopic gradient of the individual cell density (Simpson et al., 2006b). Sherratt's model predicts that two opposingly directed invasion waves, as shown in Fig. 1, come together and a well-defined boundary develops which acts to separate the two cell types. This boundary moves as a travelling wave under particular conditions (Sherratt, 2000). The key feature of this model is the formation of a localised transition zone where the two cell types come together. Cell mixing is limited to this transition zone rather than across the entire domain.

The interacting species invasion models that we have previously considered were used in conjunction with experimental observations to investigate the organisation of cell proliferation along the longitudinal axis of an invasion wave (Simpson et al., 2006b, 2007). This previous work considered short-term simulations for a limited range of geometries, parameters and initial conditions and did not focus on coalescence processes. This new analysis significantly extends the previous work by focusing on the details of coalescence processes by thoroughly characterising both the short- and long-time behaviour for a wide range of initial conditions, parameters and geometries.

Different theoretical approaches have been taken to represent similar problems in other fields. For example, Witelski (1995, 1997) considered the short-time behaviour of coalescing populations as well as detailed analyses of segregation dynamics. Cavazzoni (2000) investigated interacting invasion models which relax to Fisher's equation under certain conditions. Painter and Sherratt (2003) considered several mechanisms that might influence motility in a mixture of two motile populations. Related problems in the context of mathematical ecology have been investigated (see Murray, 2003, for a review); for example, Dunbar (1984) analysed models of pursuit and evasion in predator–prey systems while Méndez et al. (2006) studied an invasion model proposed by Cook.

1.2. Biological motivation

Our recent modelling has been aimed at simulating the development of the ENS during vertebrate embryogenesis. This process involves neural crest cells (NCC) invading the developing gut tissue as a rostro-caudal wave (Allan and Newgreen, 1980; Burns et al., 2002; Young et al., 2004). NCCs are motile and proliferate to a carrying capacity density. These cells invade the gut tissue as a constant speed invasion wave and differentiate into neurons and glia to form the ENS which gives rise to normal gut function and peristaltic contraction (Burns, 2005; Hearn et al., 1998; Young et al., 2001, 2004). Failure of the invasion process results in Hirschsprung's Disease, a relatively common and potentially fatal birth defect in humans, where a variable length of the terminal intestine fails to produce peristalsis due to the absence of the ENS.

A novel characteristic of normal ENS development is the absence of NCC death during the invasion process (Gianino et al., 2003; Young et al., 2004). This means that net increase in NCC population size is a result of birth processes only rather than a net combination of birth and death processes.

The behaviour of interacting NCC invasion waves was experimentally investigated by Burns et al. (2002) where observations were made of the long-term interaction of opposingly directed NCC invasion waves. A schematic of Burns' observations is given in Fig. 2. Burns' experimental procedure involved taking a group of NCCs from the rostral end of the embryo and grafting them at the caudal end of the developing intestine. This resulted in the indigenous NCCs invading the gut in the usual rostral-to-caudal direction while the grafted donor NCCs simultaneously invaded the gut in the opposing caudal-to-rostral direction. Burns' experiments were *in ovo*, meaning that the developing embryo was left intact after the graft took place. Consequently, the system was studied for a longer time than would be possible in an organ culture experiment (Simpson et al., 2006b, 2007).

Burns' experimental results show that two opposingly directed NCC invasion waves came together at some particular location and then each cell type continued to move in opposing directions beyond the point of intersection. This results in the two cell populations becoming widely mixed over a long period of time. This mixing phenomenon is not predicted by Sherratt's (2000) model. Therefore, we propose a different approach to capture the invasion and mixing processes. Another feature of Burns' experiments is that the gut tissues are growing simultaneously as the cell invasion process proceeds. Although it is possible to include domain growth (Landman et al., 2003; Simpson et al., 2006a) our analysis will focus on a nongrowing domain; we leave the extension to the growing case for future analysis.

To make progress in simulating coalesence phenomena we use a continuum approach and pose two conservation equations, one for each cell type. Each cell type will be motile and proliferative (Simpson et al., 2007). A general diffusive flux rule is assumed to govern the cell motility

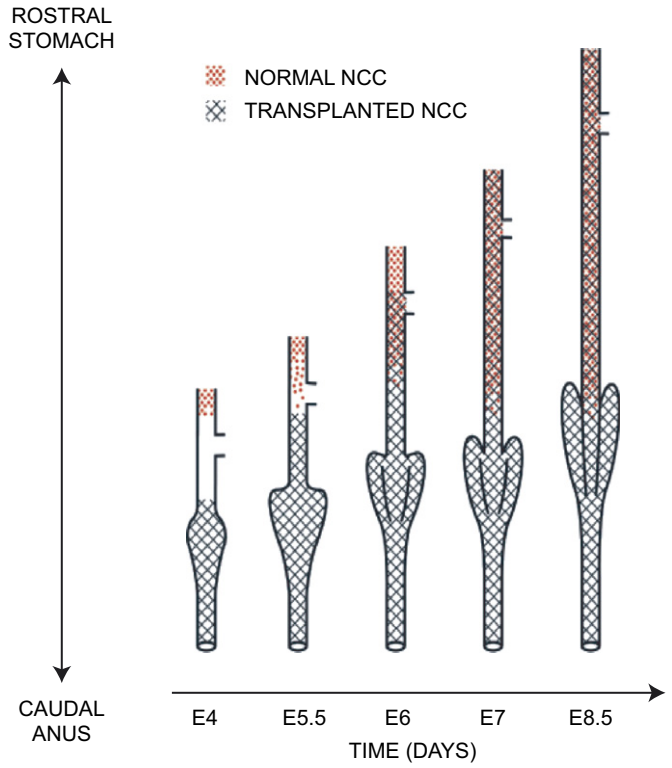

Fig. 2. Schematic diagram showing the long-term behaviour of NCC invasion adapted from Burns et al. (2002) (reproduced with permission from The Company of Biologists). Profiles are shown from E4 (embryonic age four days) to E8.5. The pattern of the rostral-to-caudal invasion is shown in red while the opposingly directed invasion of transplanted cells is shown in black. The two populations are separated at early times and continue to move in opposing directions until the end of the experiment. As the experiment proceeds the gut continues to elongate and develop symmetric cecal lobes.

while proliferation is modelled by a carrying capacity-limited logistic term. These assumptions have been shown to replicate critical features of NCC invasion in organ culture (Simpson et al., 2006b, 2007). The key feature of our model, which makes the solution very different from those considered by Sherratt (2000), is that the motility of each cell type is proportional to the macroscopic gradient of each cell density and not the gradient of the total cell density.

The transient and steady-state solutions of this model are considered. We describe and analyse various properties of these solutions. The steady solutions correspond to the long-term outcome of a developmental process.

2. Mathematical model

Conservation of mass statements are developed for two interacting cell populations with cell densities $u'(x',t')$ and $v'(x',t')$. The spatial coordinate is x' and t' is time. Cells are diffusively motile and proliferate logistically so that the long-term total cell density $u'(x',t')+v'(x',t')$ approaches a carrying capacity density denoted as c. This gives

$$\frac{\partial u'}{\partial t'} = D_u \frac{\partial}{\partial x'}\left[f\left(\frac{u'}{c},\frac{v'}{c}\right)\frac{\partial u'}{\partial x'}\right] + \lambda_u u'\left[1-\frac{u'+v'}{c}\right], \quad (1)$$

$$\frac{\partial v'}{\partial t'} = D_v \frac{\partial}{\partial x'}\left[g\left(\frac{u'}{c},\frac{v'}{c}\right)\frac{\partial v'}{\partial x'}\right] + \lambda_v v'\left[1-\frac{u'+v'}{c}\right], \quad (2)$$

where D_u and D_v are the cell diffusivities while λ_u and λ_v are the mitotic indices (proliferation rates) for the u' and v' populations, respectively. The functions $f(u'/c, v'/c)$ and $g(u'/c, v'/c)$ are unspecified linear or nonlinear dimensionless diffusivity functions. It is convenient to scale (1)–(2) with the length and time scales L and T so that $u = u'/c$, $v = v'/c$, $t = t'/T$ and $x = x'/L$. Choosing $T = 1/\lambda_u$ and $L = \sqrt{D_u/\lambda_u}$ gives the dimensionless system

$$\frac{\partial u}{\partial t} = \frac{\partial}{\partial x}\left[f(u,v)\frac{\partial u}{\partial x}\right] + u(1-u-v), \quad (3)$$

$$\frac{\partial v}{\partial t} = \mathscr{D}\frac{\partial}{\partial x}\left[g(u,v)\frac{\partial v}{\partial x}\right] + \mathscr{L}v(1-u-v), \quad (4)$$

where $\mathscr{D} = D_v/D_u$ and $\mathscr{L} = \lambda_v/\lambda_u$. The parameters $\mathscr{D}$ and $\mathscr{L}$ can be interpreted as the motility and proliferation rate of the v population relative to the u population, respectively.

For the case where both cell populations are identical, $f(u,v) = g(u,v)$, $\mathscr{D} = 1$ and $\mathscr{L} = 1$. Then Eqs. (3) and (4) can be added to arrive at an equivalent equation for the total population $w = u + v$, written as

$$\frac{\partial w}{\partial t} = \frac{\partial}{\partial x}\left[f(u,v)\frac{\partial w}{\partial x}\right] + w(1-w). \quad (5)$$

For the special case of linear diffusion with $f(u,v) = 1$, (5) is the dimensionless Fisher equation (Fisher, 1937; Murray, 2002).

2.1. Steady-state solutions

The u and v solutions will be obtained on $0 < x < L$, with no-flux conditions for both species at both boundaries, and a nonzero initial condition. We are interested in determining the nonzero steady-state solutions u_s and v_s to (3)–(4). In general, the steady solutions are spatially invariant and satisfy $u_s + v_s = 1$. However, the specific values of u_s and v_s cannot be determined *a priori*; therefore, it is not clear which proportion of each cell type will be present under steady conditions. This is a novel feature of this system. The only method to determine u_s and v_s is to determine the transient solutions and observe how they evolve through time. This property is encountered in other cell migration models (Denman et al., 2007) as well as various other applications including theoretical ecology (Shigesada, 1980) and polymer dynamics (Cohen et al., 1995). For the interacting invasion wave problem the governing equations will be integrated numerically. We are interested in how u_s and v_s depend on $\mathscr{D}$, $\mathscr{L}$, $f(u,v)$ and $g(u,v)$ as well as the initial conditions.

To quantify the relative proportion of each cell population under steady conditions we introduce a ratio, given by

$$R = \frac{u_s}{v_s}. \tag{6}$$

All numerical results will be reported in terms of R.

In many studies of cell invasion it is possible to find approximate solutions by, for example, reducing the governing equations to ordinary differential equations with a travelling wave coordinate transformation (Landman et al., 2005; Sherratt, 2000; Simpson et al., 2006b). For this particular problem, our results show that the usual travelling wave approximation, phase plane analyses and perturbation approximations are not relevant. Other attempts to obtain approximate closed form solutions have not been successful. Therefore, we rely primarily on numerical simulation together with some theoretical analysis of the solution properties.

2.2. Interpretation of the logistic terms

We now discuss the interpretation of the logistic terms in the absence of any spatial dependence. In a single species model of cell invasion governed by logistic processes, the scaled source/sink term is written as $\mathrm{d}w/\mathrm{d}t = w(1-w)$, where w is the cell density. There are two ways to interpret this model. Firstly, the model can be written as

$$\frac{\mathrm{d}w}{\mathrm{d}t} = \underbrace{w}_{\text{birth}} - \underbrace{w^2}_{\text{death}}, \tag{7}$$

where the growth is interpreted as a net combination of birth and death processes acting simultaneously. Secondly, the logistic term describes the per capita time rate of change of the population density as

$$\frac{1}{w}\frac{\mathrm{d}w}{\mathrm{d}t} = (1-w). \tag{8}$$

This quantity decreases as the cell density increases. We interpret this to be a birth process when $w<1$, or a death process when $w>1$, rather than a net combination of both acting simultaneously.

The scaled source/sink terms in the invasion models (3)–(4) have the form $\mathrm{d}u/\mathrm{d}t = u(1-w)$ and $\mathrm{d}v/\mathrm{d}t = \mathscr{L}v(1-w)$ where the total cell density is given by $w = u+v$. We interpret these source/sink terms as a per capita time rate of change of population density, as either a pure birth or pure death process.

(1) When $w<1$, the system is uncrowded and the source/sink terms are positive. In this case we interpret the logistic terms as representing cell birth processes only.
(2) When $w>1$, the system is crowded and the source/sink terms are negative. In this case we interpret the logistic terms as representing cell death processes only.

This interpretation of the logistic terms is consistent with known properties of NCC invasion. As stated previously, under normal conditions there is no cell death associated with NCC invasion (Gianino et al., 2003; Young et al., 2004). Therefore, the net increase in NCC population size is governed by birth processes only rather than a net combination of birth and death processes acting simultaneously.

3. Numerical simulation

System (3)–(4) will be simulated where the two populations are initially separated and then allowed to invade the empty region between them (Fig. 1). Both the transient and long-term behaviour will be determined repeatedly for a range of $\mathscr{D}$, $\mathscr{L}$, $f(u,v)$ and $g(u,v)$. To accurately and efficiently achieve this we will use a finite difference spatial discretisation with a second-order implicit automatic time stepping algorithm described by Sloan and coworkers (Kavetski et al., 2002; Sloan and Abbo, 1999).

The automatic time stepping algorithm detects regions of the solution requiring small time steps to reduce temporal truncation errors to an acceptable level. The algorithm also allows larger more economical steps to be taken where the solution varies more gradually in time. This is essential for the current problem as we expect periods of both slow and rapid temporal changes. Simulating long-term phenomena for a range of parameters with a heuristic time stepping algorithm could be very inefficient. The details of the numerical algorithm are given in Appendix A.

4. Analysis

It is possible to analyse certain properties of the transient and steady-state solutions of (3)–(4). A linear stability analysis shows that the steady-state solution, $u_s + v_s = 1$, is stable against small nonuniform perturbations. This applies to both linear and nonlinear diffusivities. Appendix B contains the details of the stability analysis.

We also develop a comparison principle and investigate certain limiting behaviours where parameters $\mathscr{D}$ and/or $\mathscr{L}$ are set to zero.

4.1. Comparison principle with $f(u,v) = g(u,v) = G(w)$

To assist describing the dynamics of system (3)–(4) we investigate special conditions where the solution can be compared with the solution of a simpler single species equation. Strong maximum principles for parabolic equations (Protter and Weinberger, 1967, p. 188) yield a comparison principle (McOwen, 1996, p. 312–313; Pao, 1992, Exercise 7) which can be applied to (3)–(4) for any initial condition satisfying $0 \leqslant u(x,0) + v(x,0) \leqslant 1$.

Consider the nonlinear differential operator F defined as

$$F[U] = \frac{\partial U}{\partial t} - \frac{\partial}{\partial x}\left[G(U)\frac{\partial U}{\partial x}\right] - U(1-U) = 0. \tag{9}$$

With $G(U) = 1$, Eq. (9) is Fisher's equation (Fisher, 1937), otherwise the equation is an extension of Fisher's equation

with nonlinear diffusivity $G(U)$ (Murray, 2002; Witelski, 1995, 1997). With no-flux boundary conditions and initial conditions satisfying $0 \leqslant U(x,0) \leqslant 1$, the solution of (9) satisfies $0 \leqslant U(x,t) \leqslant 1$ for all x and $t > 0$ provided that $G'(U)$ is bounded (Protter and Weinberger, 1967).

Defining $w = u + v$ and setting $\mathscr{D} = 1$, Eqs. (3) and (4) can be added to produce a single equation in w, as long as $f(u,v) = g(u,v)$ and $f(u,v) = G(w)$. This gives

$$\frac{\partial w}{\partial t} - \frac{\partial}{\partial x}\left[G(w)\frac{\partial w}{\partial x}\right] - w(1-w) + (1-\mathscr{L})v(1-w) = 0. \tag{10}$$

For $0 \leqslant \mathscr{L} \leqslant 1$, $(1-\mathscr{L})v(1-w) \geqslant 0$ for all $w \leqslant 1$. Therefore, the following inequality can be formed:

$$\begin{aligned} 0 &= \frac{\partial w}{\partial t} - \frac{\partial}{\partial x}\left[G(w)\frac{\partial w}{\partial x}\right] - w(1-w) + (1-\mathscr{L})v(1-w) \\ &\geqslant \frac{\partial w}{\partial t} - \frac{\partial}{\partial x}\left[G(w)\frac{\partial w}{\partial x}\right] - w(1-w) = F[w]. \end{aligned} \tag{11}$$

Combining (9) and (11) gives the comparison

$$F[U] \geqslant F[w]. \tag{12}$$

If $U(x,0) \geqslant w(x,0) \geqslant 0$ for all x and both U and w satisfy no-flux boundary conditions, then the comparison principle yields that $U(x,t) \geqslant w(x,t)$ for all x and $t > 0$. In addition, since $0 \leqslant U(x,t) \leqslant 1$, we obtain the important result that $0 \leqslant w(x,t) = u(x,t) + v(x,t) \leqslant 1$ for all x and t. Therefore, when $\mathscr{D} = 1$ with $f(u,v) = g(u,v) = G(w)$, the solution to (3)–(4) will be restricted to $0 \leqslant u(x,t) + v(x,t) \leqslant 1$ for all x and $t > 0$. This comparison principle applies to arbitrary initial conditions satisfying $0 \leqslant u(x,0) + v(x,0) \leqslant 1$, and an arbitrary domain. We will make use of this result in Section 5 to interpret numerical simulations.

By symmetry, these arguments also apply when $\mathscr{L} > 1$, since the scaling in (1)–(2) could have been constructed relative to the v parameters, rather than the u parameters. This comparison principle has been developed for the special case where the nonlinear diffusivity is written as a function of the total cell density $f(u,v) = G(w)$. Other functional forms are possible; using numerical results in Section 5 we conjecture that the comparison principle also applies to other forms provided that $f(u,v) = g(u,v)$.

It does not appear possible to develop a comparison principle when $\mathscr{D} \neq 1$ to yield a condition to be met for $u(x,t) + v(x,t) > 1$. For this case we rely on numerical simulations.

The arguments outlined above also apply to more general logistic-type source terms (Tsoularis and Wallace, 2002). For example, the same result can be obtained when the source term in Eq. (9) and the analogous source terms in (3)–(4) are replaced with terms like $U^m(1-U)$ where m is a positive integer.

4.2. Steady-state solutions with $\mathscr{D} = 0$ and/or $\mathscr{L} = 0$

Setting $\mathscr{D} = 0$ and $\mathscr{L} = 0$ in (3)–(4) means that the v population is immotile and nonproliferative. The governing equation for the v population is $\partial v/\partial t = 0$ and so the initial condition for v cannot evolve with time. The resulting steady states are not spatially uniform and this case is not considered any further.

Setting $\mathscr{D} = 0$ in (3)–(4) means that the v population is immotile but proliferative. Regardless of the value of $\mathscr{L}$, the steady solution is $u_s + v_s = 1$ with $u_s = 1$ and $v_s = 0$. Therefore, $R = \infty$ for this case.

For $\mathscr{L} = 0$ and any $\mathscr{D} > 0$, the value of R can be determined. Setting $\mathscr{L} = 0$ implies that the v population is nonproliferative but motile. Under these conditions the mass of v, $m_v = \int_0^L v(x,t)\,\mathrm{d}x$, is conserved for all $t > 0$. Therefore, at steady state, this mass will be uniformly distributed giving $v_s = m_v/L$. Consequently $u_s = 1 - m_v/L$.

5. Results and discussion

A detailed series of results are presented for linear diffusion. Following these, further results for other common choices of cell diffusivity functions are presented and discussed.

5.1. Linear diffusion: transient solutions

To simulate coalescence with linear diffusion we set $f(u,v) = g(u,v) = 1$. Transient profiles are considered before analysing the steady solutions. Profiles are generated on $0 < x < 10$ with the two cell populations being initially separated. We consider

$$u(x,0) = 1 - H(x-2), \quad v(x,0) = H(x-8), \tag{13}$$

where H is the Heaviside step function. Further scenarios with different domains and initial conditions are investigated in later sections.

Results for identical cell populations with $\mathscr{D} = \mathscr{L} = 1$ are summarised in the first column of Fig. 3 where solutions are shown for a range of times required for the initial condition to evolve into the steady solution. The u and v cell populations, initially separate, rapidly invade the unoccupied space $2 < x < 8$. The cell populations coalesce symmetrically at $x = 5$. After $t = 5$ the sum of the populations is approximately $u + v = 1$ for all $0 < x < 10$. Therefore, for $t > 5$ the proliferation terms in (3)–(4) are small. However, the spatial gradients in u and v are nonzero so that the macroscopic profiles of $u(x,t)$ and $v(x,t)$ continue to evolve in time until $\partial u/\partial x = \partial v/\partial x = 0$. For long-term conditions as $t \to \infty$, the steady-state solution is $u_s = v_s = 0.5$. This result is intuitively expected since both cell types are identical and the initial conditions are symmetric.

Transient solutions where the two cell types have different motilities and proliferation rates ($\mathscr{D} \neq 1$ and $\mathscr{L} \neq 1$) are also demonstrated. The same initial conditions

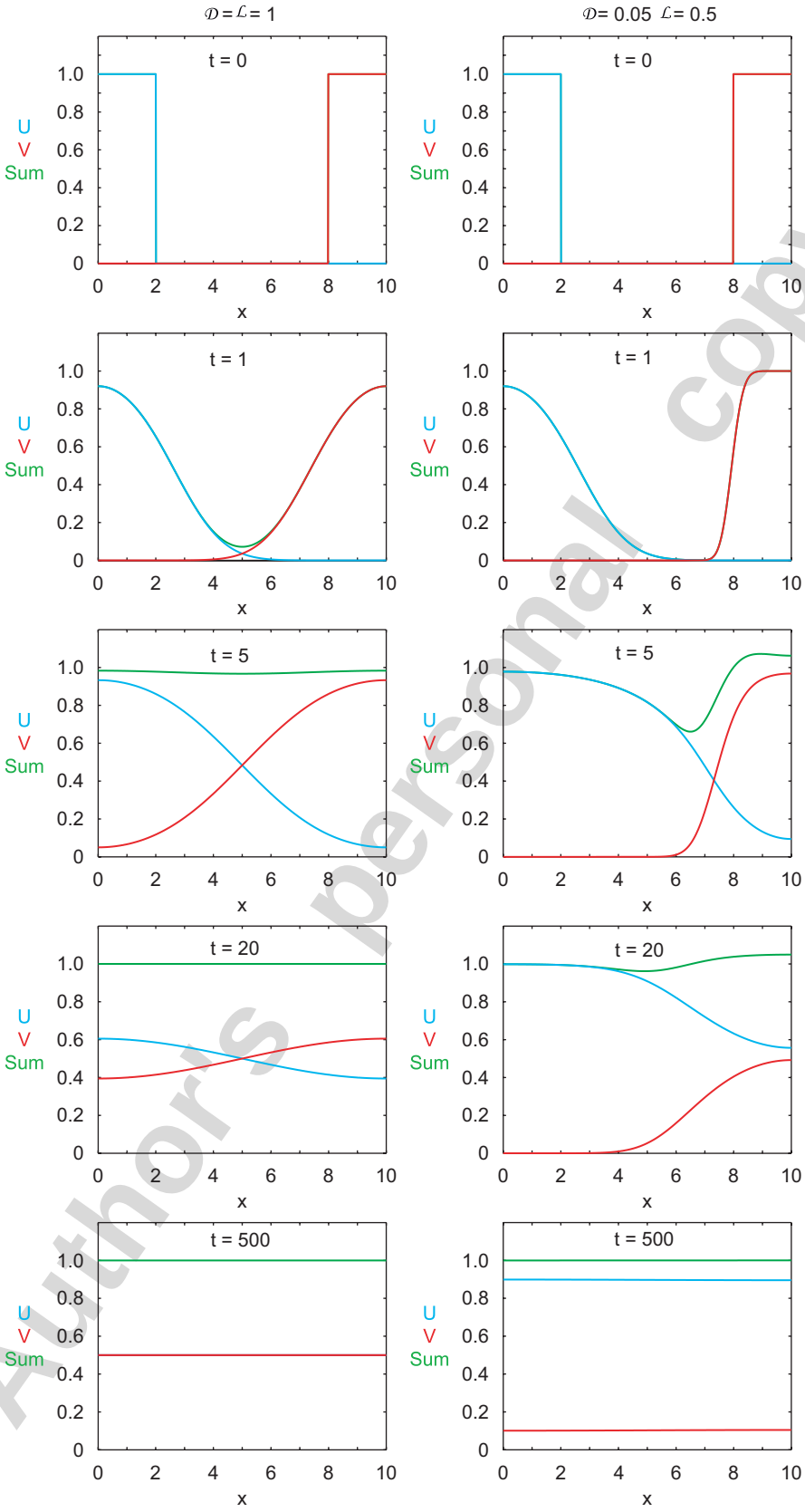

Fig. 3. Temporal evolution of coalescence with linear diffusion. Results are shown for identical populations $\mathcal{D} = \mathcal{L} = 1$ in the left hand column at $t = 0, 1, 5, 20$ and 500. Details of the $u(x, t)$ (blue), $v(x, t)$ (red) and the sum $u(x, t) + v(x, t)$ (green) are shown. Equivalent results are shown in the right-hand column for $\mathcal{D} = 0.05$ and $\mathcal{L} = 0.5$. Numerical simulations are evaluated with $\Delta x = 0.01$ and variable Δt.

are considered with $\mathscr{D} = 0.05$ and $\mathscr{L} = 0.5$. These parameters imply that the u population is 20 times more motile and twice as proliferative than the v population. Transient solutions are given in the second column of Fig. 3. The transient profiles reflect that the u population is more invasive than the v population, as the u profile advances to the right more rapidly than the v profile advances to the left. The same steady state $u_s + v_s = 1$ is achieved. However, the steady profile consists of more u cells than v cells with $u_s = 0.897$ and $v_s = 0.103$. This agrees with our intuitive notion that their ought to be more u cells than v cells as the u population is more motile and proliferative. This computation is repeated for a range of $\mathscr{D}$ and $\mathscr{L}$ values.

5.2. Linear diffusion: steady-state solutions

It is unclear how the proportion of u_s and v_s varies with $\mathscr{D}$, $\mathscr{L}$ or with the initial conditions. For example, $R = 1$ for $\mathscr{D} = \mathscr{L} = 1$ while $R = 8.71$ for $\mathscr{D} = 0.05$ and $\mathscr{L} = 0.5$. The ratio R is reported in Fig. 4a as a function of $\mathscr{D}$ and $\mathscr{L}$ for $0 \leqslant \mathscr{L} \leqslant 10$ and $0.05 \leqslant \mathscr{D} \leqslant 5$ with the symmetric initial condition (13). All profiles pass through $R = 4$ for $\mathscr{L} = 0$ since $m_v = 2$ for the initial condition (13); accordingly $v_s = 0.2$ and $u_s = 0.8$ for any $\mathscr{D}$.

The profiles in Fig. 4a show that $R = R(\mathscr{D}, \mathscr{L})$. Several properties of this function can be deduced.

(1) For sufficiently large fixed $\mathscr{D}$, the profiles are monotonically decreasing functions of $\mathscr{L}$, that is $\partial R/\partial \mathscr{L} < 0$ for all $\mathscr{L}$.
(2) For sufficiently small fixed $\mathscr{D}$, the profiles are increasing functions of $\mathscr{L}$ ($\partial R/\partial \mathscr{L} > 0$) for sufficiently small $\mathscr{L}$ and the profiles are decreasing functions of $\mathscr{L}$ ($\partial R/\partial \mathscr{L} < 0$) for sufficiently large $\mathscr{L}$.
(3) For each fixed $\mathscr{L}$, R is a monotonically decreasing function of $\mathscr{D}$, that is $\partial R/\partial \mathscr{D} < 0$ for all $\mathscr{D}$.

On intuitive grounds, some of these trends are expected. For example, since increasing the value of $\mathscr{L}$ means that the relative proliferation rate of the v population to the u population increases, we anticipate that the relative number of v cells will increase, giving rise to a smaller value of R. However, this argument is not valid for all $\mathscr{L}$ values, since it is false when the relative motility of the v to the u population, given by $\mathscr{D}$, is sufficiently small. The reason for this is not obvious. Alternatively, as the relative motility of the v to the u population decreases, we anticipate the proportion of v cells will decrease, corresponding to a increase in R. This result appears to be independent of $\mathscr{L}$.

From Fig. 4a, we can deduce the regions in the $(\mathscr{D},\mathscr{L})$ parameter space where $R < 1$ and $R > 1$. Fig. 5 illustrates this bifurcation diagram. For values of $\mathscr{L} > \mathscr{L}(\mathscr{D})$, $R < 1$, while for $\mathscr{L} < \mathscr{L}(\mathscr{D})$, $R > 1$. Hence, we can readily determine whether u_s dominates over v_s.

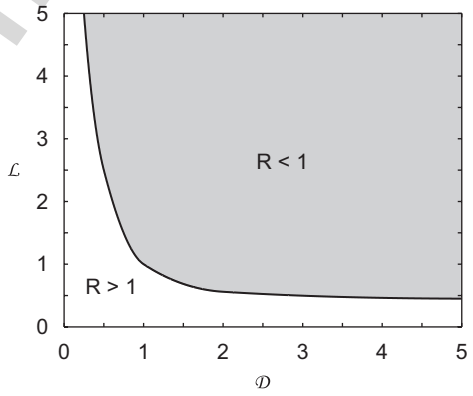

Fig. 5. Bifurcation diagram for the steady-state solution with linear diffusion and symmetric initial conditions (13). The curve corresponding to $R = 1$ is plotted in the $(\mathscr{D},\mathscr{L})$ parameter space, and the region corresponding to $R < 1$ is shaded while the region corresponding to $R > 1$ is unshaded.

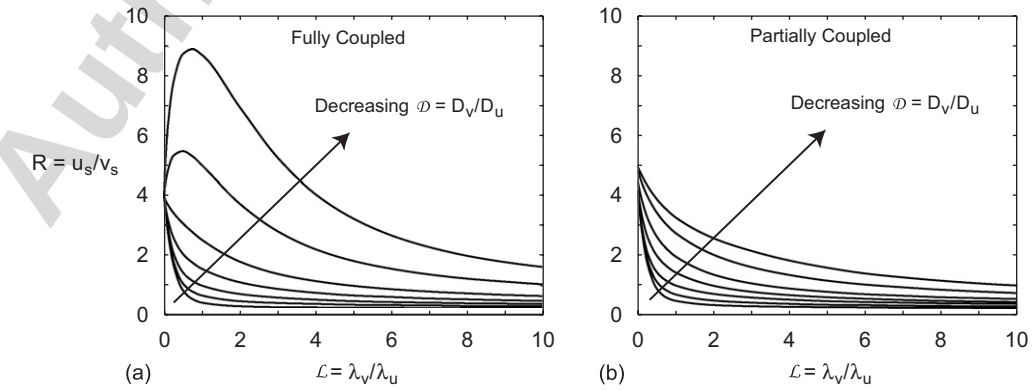

Fig. 4. Values of $R = u_s/v_s$ versus $\mathscr{L}$ for linear diffusion and the symmetric initial condition (13) showing (a) fully coupled conditions and (b) partially coupled conditions. Seven contours are shown for $\mathscr{D} = 0.05, 0.1, 0.25, 0.5, 1.0, 2.0$ and 5.0.

We now focus our attention on investigating the reasons for the increasing R profiles for sufficiently small $\mathscr{D}$ and $\mathscr{L}$. To do this, we compare the transient evolution of the solution for $\mathscr{D}=\mathscr{L}=1$ and $\mathscr{D}=0.05$ and $\mathscr{L}=0.5$ (Fig. 3). Two obvious differences are revealed. Firstly, when the coefficients are less than unity the u population invades the empty space more rapidly than the v population, giving rise to a nonsymmetric coalescence pattern. Secondly, the rapid invasion is associated with the local cell density in the region of coalescence rising above capacity density; that is $u(x,t)+v(x,t)>1$ for some period of time, as illustrated in Fig. 3 in the region $8<x<10$ at $t=5$. Comparing the $u+v$ profiles shows that the total cell density never rises above unity for the $\mathscr{D}=\mathscr{L}=1$ case.

The formation of a region where the total cell density in greater than the capacity density means that overcrowding occurs and the logistic proliferation terms in (3)–(4) become negative. With our interpretation of the logistic terms given in Section 2.2, this overcrowding leads to cell death. Therefore, it seems reasonable to conjecture that overcrowding occurs for some values of $\mathscr{D}$ and $\mathscr{L}$ considered in Fig. 4a, while no overcrowding occurs for other values. This provides a potential explanation for the differences in behaviour of R as a function of $\mathscr{L}$, depending on the size of $\mathscr{D}$ (Fig. 4a).

5.2.1. Linear diffusion: role of overcrowding and cell death

To better understand the role of overcrowding in determining the steady-state solutions, we resimulate all results in Fig. 4a under modified conditions where cell death processes are eliminated. This is achieved by introducing a switch function, $\chi(u+v)$, which leads to a modified system given by

$$\frac{\partial u}{\partial t}=\frac{\partial}{\partial x}\left[f(u,v)\frac{\partial u}{\partial x}\right]+\chi(u+v)u[1-(u+v)], \tag{14}$$

$$\frac{\partial v}{\partial t}=\mathscr{D}\frac{\partial}{\partial x}\left[g(u,v)\frac{\partial v}{\partial x}\right]+\chi(u+v)\mathscr{L}v[1-(u+v)]. \tag{15}$$

The switch function $\chi(u+v)$ must not affect the system in uncrowded conditions. This is achieved by setting $\chi(u+v)=1$ when $(u+v)\leqslant 1$ so that birth processes will proceed unhindered in uncrowded regions. The switch function $\chi(u+v)$ will be used to inactivate death processes. This is achieved by setting $\chi(u+v)=0$ when $(u+v)>1$ meaning that death processes will be inactivated. In summary, the switch function eliminates cell death processes while having no affect on cell birth. The switch is defined as,

$$\chi(u+v)=H[1-(u+v)]=\begin{cases}1, & (u+v)\leqslant 1,\\ 0, & (u+v)>1.\end{cases} \tag{16}$$

We will refer to simulations conducted without the switch as "fully coupled". Simulations conducted with the switch are "partially coupled" since the switch overrides and partly removes the coupling for crowded conditions. Making comparisons of these kinds of coupled and partially coupled solutions have been used previously to determine the relative importance of complex coupling processes in models of variable density fluid flow (Simpson and Clement, 2003, 2004). This switch is similar to the mechanism introduced by Hillen and Painter (2001) who turned off a chemotactic response at high cell densities to study long-term behaviour of chemotactic cell migration models.

If the partially coupled and fully coupled steady-state solutions are different for the same parameters and initial conditions, then overcrowding and cell death must have occurred during the fully coupled simulation. On the other hand, if the steady-state solutions are the same, we cannot deduce whether cell death occurred from R alone. In this case the fully coupled transient profile must be studied to see whether $u(x,t)+v(x,t)>1$ in any region for some time. However, for conditions where overcrowding never occurs in the fully coupled solution, the steady state fully and partially coupled R values must be identical.

To understand how important overcrowding is, all fully coupled simulations in Fig. 4a were repeated under partially coupled conditions and the corresponding R values are given in Fig. 4b. The most striking effect of introducing the $\chi(u+v)$ switch is that all R profiles are decreasing functions of $\mathscr{L}$, that is $\partial R/\partial\mathscr{L}<0$ for all $\mathscr{L}$. This means that the formation of monotonically increasing regions in the fully coupled profiles (Fig. 4a) must be associated, in some way, with conditions that allow overcrowding. The other key feature of the partially coupled profiles is that the curves do not pass through the common point $R=4$ for $\mathscr{L}=0$. The steady-state solution of the partially coupled problem does not satisfy $u_s+v_s=1$, rather the solution is $u_s+v_s=K$ for some constant $K\geqslant 1$.

To quantitatively assess the influence of cell death, the R values in Fig. 4a and 4b are compared. This shows that all values of R are different between the fully and partially coupled simulations except when $\mathscr{D}=1$ regardless of $\mathscr{L}$. This outcome is in accordance with the comparison principle which showed that overcrowding will never occur for $f(u,v)=g(u,v)=G(w)$ and $\mathscr{D}=1$ provided that $0\leqslant u(x,0)+v(x,0)\leqslant 1$. Unfortunately, the comparison principle provides no information when $\mathscr{D}\neq 1$. In Section 5.2, we hypothesised that overcrowding might only occur for sufficiently small $\mathscr{D}$ and sufficiently small $\mathscr{L}$ corresponding to the profiles in Fig. 4a that had a positive slope. Quantitatively comparing the coupled and partially coupled simulations shows that this supposition is incorrect as overcrowding occurs whenever $\mathscr{D}\neq 1$.

5.3. Linear diffusion: nonsymmetric initial conditions and large domains

Further simulations will be conducted for different initial conditions and a wider domain to demonstrate that the comparison principle applies to more general problems.

A special feature of the previous example was that $u(x,0)$ and $v(x,0)$ were spatially symmetric. A more general case is considered with a nonsymmetric initial condition. We change the initial distribution of u to

$$u(x,0) = 1 - H(x-l), \quad v(x,0) = H(x-8). \tag{17}$$

Results are generated for $l = 3$. The temporal profiles for this initial condition are similar to those shown in Fig. 3 and so only the steady profiles for R are presented. Fully coupled and partially coupled steady profiles are given in Fig. 6.

All simulations presented so far are relevant for a narrow domain. Many invasion models support travelling wave solutions valid on $-\infty < x < \infty$ (Maini et al., 2004a,b; Murray, 2002; Sherratt, 2000). To observe travelling waves numerically, simulations must be performed on wide domains. To observe travelling wave-type behaviour we consider (3)–(4) on $-50 < x < 50$ with

$$u(x,0) = \frac{1}{1+\exp(x-\alpha_u)}, \quad v(x,0) = \frac{1}{1+\exp(\alpha_v - x)}. \tag{18}$$

The exponential initial conditions are chosen since they evolve into travelling wave-type solutions faster than Heaviside initial conditions. A widely separated symmetric initial distribution of u and v is specified by setting $\alpha_u = -30$ and $\alpha_v = 30$. We expect that there will be sufficient space between the populations so that travelling wave-like profiles will form during the transient phase. The temporal evolution of the system with $\mathscr{D} = \mathscr{L} = 1$ and $\mathscr{D} = 0.05$ and $\mathscr{L} = 0.5$ is shown in Fig. 7. The R values are given in Fig. 8.

Comparing the fully and partially coupled R values for the nonsymmetric initial condition (Fig. 6) and the wide domain (Fig. 8) reveals how important overcrowding and cell death is for various $\mathscr{D}$ and $\mathscr{L}$. All fully coupled R values are different to the partially coupled R values with the exception of the $\mathscr{D} = 1$ case. This result is anticipated from the comparison principle which is valid for arbitrary initial conditions satisfying $0 \leqslant u(x,0) + v(x,0) \leqslant 1$ and an arbitrary domain.

Although the results presented so far yield complex and interesting behaviour, they are limited to a special case of linear diffusion. Many applications of continuum modelling in mathematical biology use a nonlinear diffusivity function to include effects of cell–cell contact and crowding on the cell motility (Cai et al., 2006; Maini et al., 2004a; Sherratt, 2000; Simpson et al., 2006b). We now resimulate some of the problems previously considered with some common choices of nonlinear diffusivity functions.

5.4. Standard nonlinear diffusivity

The suitability of linear diffusion has been questioned by several authors within the context of representing cell motility (Cai et al., 2006; Sherratt, 2000). A further suite of numerical results will be generated for two common choices of $f(u,v)$ and $g(u,v)$ in (3)–(4).

Increasing degenerate nonlinear diffusion is the most commonly adopted nonlinear diffusivity form in cell migration applications. Here, we consider

$$f(u,v) = g(u,v) = (u+v)^n \tag{19}$$

with $n > 0$. Sharp fronted solutions are expected since $f(u,v) = g(u,v) = 0$ when $u + v = 0$. Other analysts (Cai et al., 2006; Painter and Sherratt, 2003; Simpson et al., 2006b) use decreasing diffusivity functions to simulate a reduced motility in high cell density regions due to cell–cell interactions. Such a diffusivity function is given by

$$f(u,v) = g(u,v) = \frac{1}{1+\kappa(u+v)}, \tag{20}$$

with $\kappa > 0$. Preliminary investigations suggest that the results are qualitatively similar for various values of n and κ. By way of example we present results for $n = \kappa = 1$.

Because the qualitative features of the results for linear diffusion were independent of the width of the domain and the initial conditions provided $0 \leqslant u(x,0) + v(x,0) \leqslant 1$, we

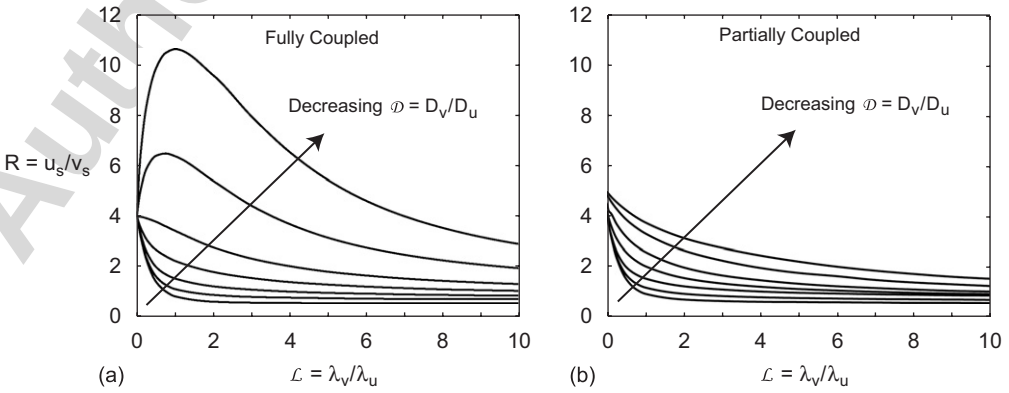

Fig. 6. Values of $R = u_s/v_s$ versus $\mathscr{L}$ for the nonsymmetric initial condition (17) showing (a) fully coupled conditions and (b) partially coupled conditions. Seven contours are shown for $\mathscr{D} = 0.05, 0.1, 0.25, 0.5, 1.0, 2.0$ and 5.0.

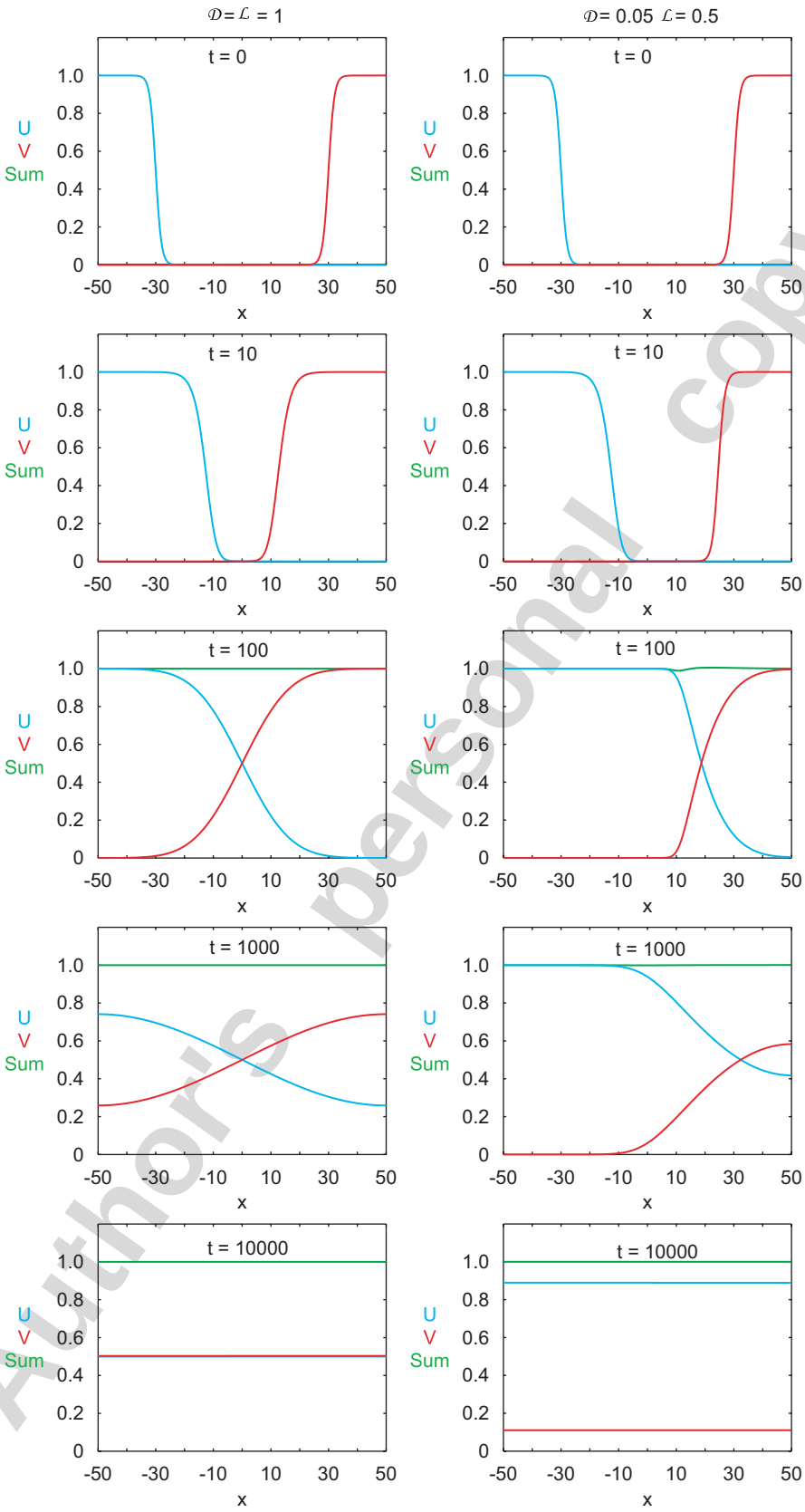

Fig. 7. Temporal evolution of coalescence with linear diffusion on the wide domain. Results are shown for identical populations $\mathcal{D} = \mathcal{L} = 1$ in the left-hand column at $t = 0, 10, 100, 1000$ and 10 000. Details of the $u(x, t)$ (blue), $v(x, t)$ (red) and the sum $u(x, t) + v(x, t)$ (green) are shown. Equivalent results are shown in the right hand column for $\mathcal{D} = 0.05$ and $\mathcal{L} = 0.5$. Numerical simulations are evaluated with $\Delta x = 0.05$ and variable Δt.

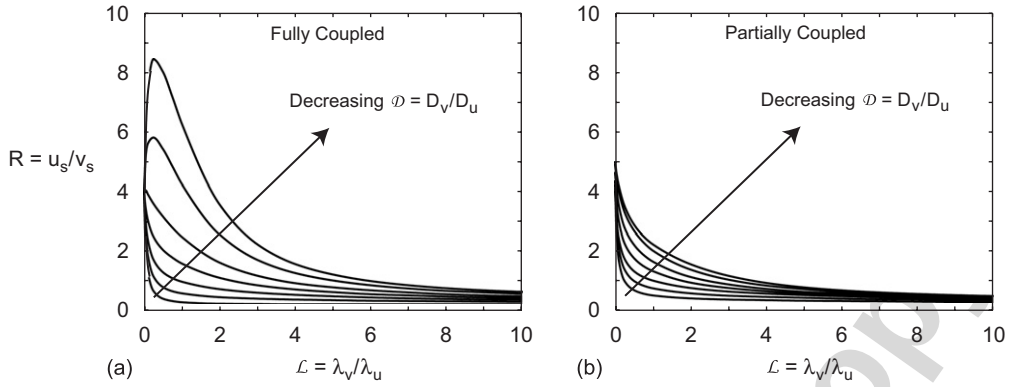

Fig. 8. Values of $R = u_s/v_s$ versus $\mathscr{L}$ for the wide domain initial condition (18) showing (a) fully coupled conditions and (b) partially coupled conditions. Seven contours are shown for $\mathscr{D} = 0.05, 0.1, 0.25, 0.5, 1.0, 2.0$ and 5.0.

will simulate nonlinear diffusivity problems with initial conditions (13) on $0<x<10$. Transient profiles are presented in Figs. 9 and 10 for the increasing and decreasing diffusivity functions, respectively. Results for identical populations $\mathscr{D} = \mathscr{L} = 1$ are presented together with equivalent results with $\mathscr{D} = 0.05$ and $\mathscr{L} = 0.5$. The most obvious difference between the linear diffusion and the nonlinear diffusion cases is that the profiles for the degenerate increasing diffusivity are sharp fronted whereas all other cases involve smooth differentiable profiles. As for linear diffusion, the identical population problems with the two nonlinear diffusivity functions evolve so that $0 \leqslant u(x,t) + v(x,t) \leqslant 1$ for all $t>0$. However, the total population density for $\mathscr{D} = 0.05$ and $\mathscr{L} = 0.5$ becomes overcrowded with $u(x,t) + v(x,t) > 1$ for some period of time.

Qualitatively similar trends for the R values are illustrated Figs. 11 and 12 for the increasing and decreasing nonlinear diffusivity functions, respectively. Comparing the coupled and partially coupled simulations shows that all R values differ between the coupled and partially coupled conditions with the exception of the $\mathscr{D} = 1$ case. Therefore, as before, overcrowding and cell death must occur during the transient evolution of all problems other than the $\mathscr{D} = 1$ case. The result for $\mathscr{D} = 1$ is anticipated from the comparison principle developed in Section 4.

5.5. Nonstandard nonlinear diffusivity

In addition to standard nonlinear diffusivities, it is prudent to test other forms suggested in the literature. As an example, the diffusivity functions proposed by Sherratt (2000), to simulate competing invasion fronts with contact inhibition, are considered. In this case $f(u,v) \neq g(u,v)$ and are given by

$$f(u,v) = \frac{u}{(u+v)}, \quad g(u,v) = \frac{v}{(u+v)}. \tag{21}$$

Sherratt used initial conditions where $u+v>0$ for all x Sherratt, 2000. Here, we simulate two populations initially separated with $u+v=0$ at $t=0$ in some region. Therefore, we apply (21) only where $u+v>0$ otherwise we set $f(u,v) = g(u,v) = 0$ wherever $u+v=0$. Initial conditions (13) are used to repeat all previous simulations on $0<x<10$. Transient profiles are given in Fig. 13. These results are radically different to all other transient profiles regarding the role of overcrowding and cell death. The solution for $\mathscr{D} = \mathscr{L} = 1$ shows that $u(x,t) + v(x,t) > 1$ in some locations at later times. In this case the comparison principle cannot be applied as (3)–(4) do not sum to produce a similar equation for the total population.

Steady-state R profiles are given in Fig. 14. These results are also remarkably different to the other results as the fully coupled R values are all different to the partially coupled R values except when $\mathscr{D} = \mathscr{L} = 1$. Therefore, Sherratt's diffusivity functions permit overcrowding for all parameters since the transient profiles in Fig. 13 show that overcrowding also occurs when $\mathscr{D} = \mathscr{L} = 1$. We conjecture that the origin of this difference is that $f(u,v) \neq g(u,v)$, which is unlike the other cases considered here.

In addition to simulating the coalescence problem with Sherratt's diffusivity functions we also conducted further simulations with a range of $f(u,v)$ and $g(u,v)$. Other cases where $f(u,v) \neq g(u,v)$ were tested, for example $f(u,v) = u$ and $g(u,v) = v$, and $f(u,v) = 1/(1+u)$ and $g(u,v) = 1/(1+v)$. For both cases the simulations revealed that cell death occurred for all values of $\mathscr{D}$ and $\mathscr{L}$.

Further simulations were conducted for diffusivities satisfying $f(u,v) = g(u,v)$ but which cannot be written as a function of the total cell density $u+v$. We considered $f(u,v) = g(u,v) = u$, v, $1+uv$ and e^{-uv}. Repeating the simulations showed that R differed between the coupled and partially coupled simulations except for the special case when $\mathscr{D} = 1$ for any $\mathscr{L}$. For all cases tested with $f(u,v) = g(u,v)$ and $\mathscr{D} = 1$, the fully coupled transient solutions never became overcrowded and $0 \leqslant u(x,t) + v(x,t) \leqslant 1$ for all $t>0$. These results suggest that the comparison principle is valid when just $f(u,v) = g(u,v)$ and the additional condition $f(u,v) = G(w)$ is unnecessary.

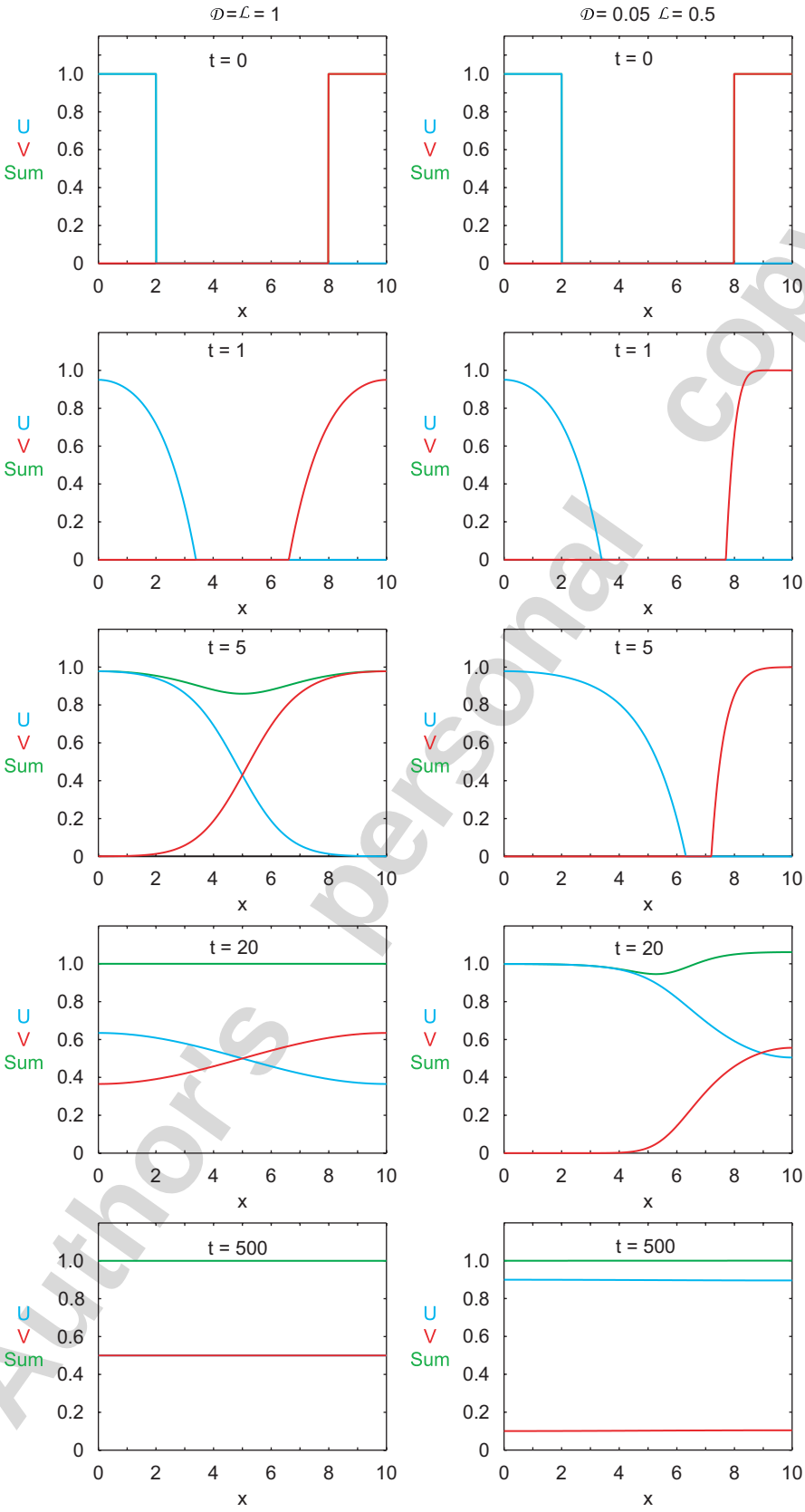

Fig. 9. Temporal evolution of coalescence with increasing degenerate nonlinear diffusion $f(u,v) = g(u,v) = (u+v)^n$ and $n = 1$. Results are shown for identical populations $\mathscr{D} = \mathscr{L} = 1$ in the left-hand column at $t = 0, 1, 5, 20$ and 500. Details of the $u(x,t)$ (blue), $v(x,t)$ (red) and the sum $u(x,t) + v(x,t)$ (green) are shown. Equivalent results are shown in the right-hand column for $\mathscr{D} = 0.05$ and $\mathscr{L} = 0.5$. Numerical simulations are evaluated with $\Delta x = 0.01$ and variable Δt.

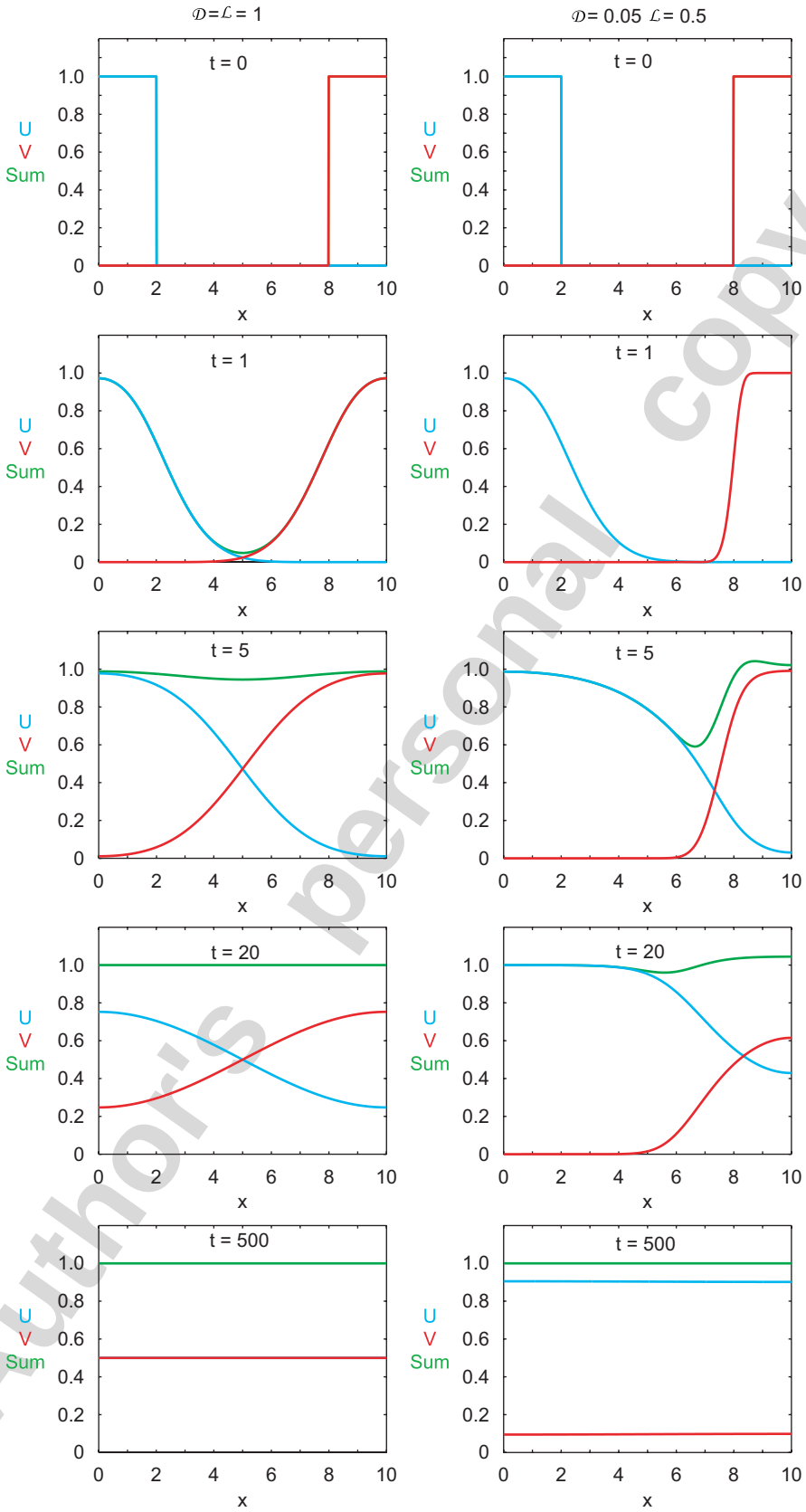

Fig. 10. Temporal evolution of coalescence with decreasing nonlinear diffusion $f(u,v)=g(u,v)=(1+\kappa(u+v))^{-1}$ and $\kappa=1$. Results are shown for identical populations $\mathscr{D}=\mathscr{L}=1$ in the left-hand column at $t=0,1,5,20$ and 500. Details of the $u(x,t)$ (blue), $v(x,t)$ (red) and the sum $u(x,t)+v(x,t)$ (green) are shown. Equivalent results are shown in the right-hand column for $\mathscr{D}=0.05$ and $\mathscr{L}=0.5$. Numerical simulations are evaluated with $\Delta x=0.01$ and variable Δt.

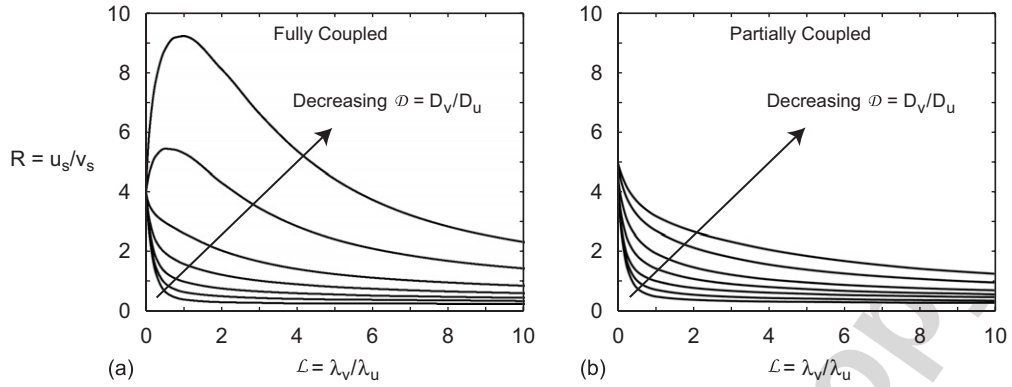

Fig. 11. Values of $R = u_s/v_s$ versus $\mathcal{L}$ for increasing degenerate nonlinear diffusivity functions with the initial condition (13) showing (a) fully coupled conditions and (b) partially coupled conditions. Seven contours are shown for $\mathcal{D} = 0.05, 0.1, 0.25, 0.5, 1.0, 2.0$ and 5.0.

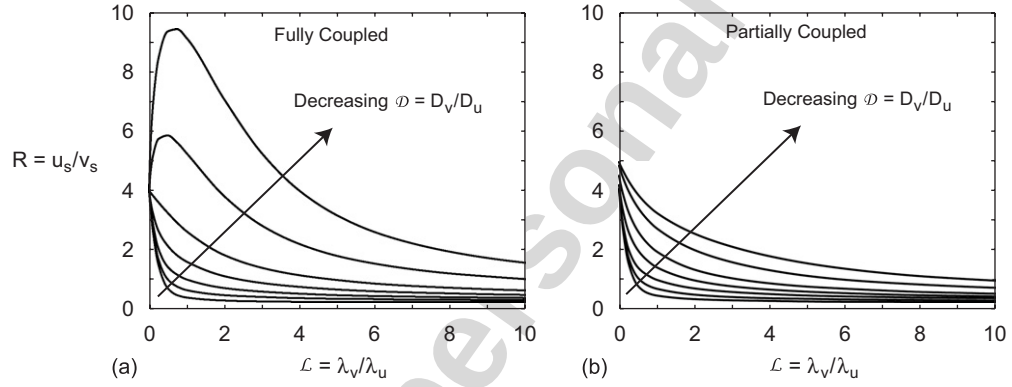

Fig. 12. Values of $R = u_s/v_s$ versus $\mathcal{L}$ for decreasing nonlinear diffusivity functions with the initial condition (13) showing (a) fully coupled conditions and (b) partially coupled conditions. Seven contours are shown for $\mathcal{D} = 0.05, 0.1, 0.25, 0.5, 1.0, 2.0$ and 5.0.

6. Conclusions

This analysis considers the transient and long-term dynamics of two invasive cell populations which undergo coalescence. The problem is modelled as a coupled reaction diffusion system with the cell motility governed by a linear or nonlinear diffusive flux and a logistic source term represents proliferation so that the long-term total cell density will approach a carrying capacity density. This model admits solutions which have the same qualitative characteristics observed in experimental assays investigating the long-term interaction of opposingly directed invasion waves. An interesting feature of the system is that the expression governing the steady-state behaviour is underdetermined so the only way to deduce the steady-state solution is to integrate the system through time.

The simulation and analysis of the coalescence patterns provide very insightful strong conclusions of interest to experimental cell biologists. If two cell populations are invasive and behave according to (3)–(4), we suggest that the long-term interaction assay performed by Burns et al. (2002) will yield important information to assist in identifying the particular mechanism(s) regarding cell motility. In addition to making observations of the spatiotemporal distributions of the cell types during and after coalescence, it would be useful to determine the presence or absence of cell death. Although cell death was not measured in Burns' original experiments (A. Burns, personal communication, 2006), other analysis of the normal rostral-to-caudal migration of NCCs revealed that cell death does not normally occur (Gianino et al., 2003; Young et al., 2004). Therefore, we suggest that in future coalescence assays it would be very useful to make similar observations of cell death. The analysis suggests that the presence or absence of overcrowding will be independent of the initial condition so long as the initial cell density is below the tissue carrying capacity. This is a positive outcome since it is very difficult to control the precise number and distribution of cells in a grafting assay.

The fully and partially coupled numerical simulations together with the comparison principle shows that if cell death is not observed in the coalescence assay then the two populations u and v have the same diffusive motility mechanism. Making such an observation would be useful

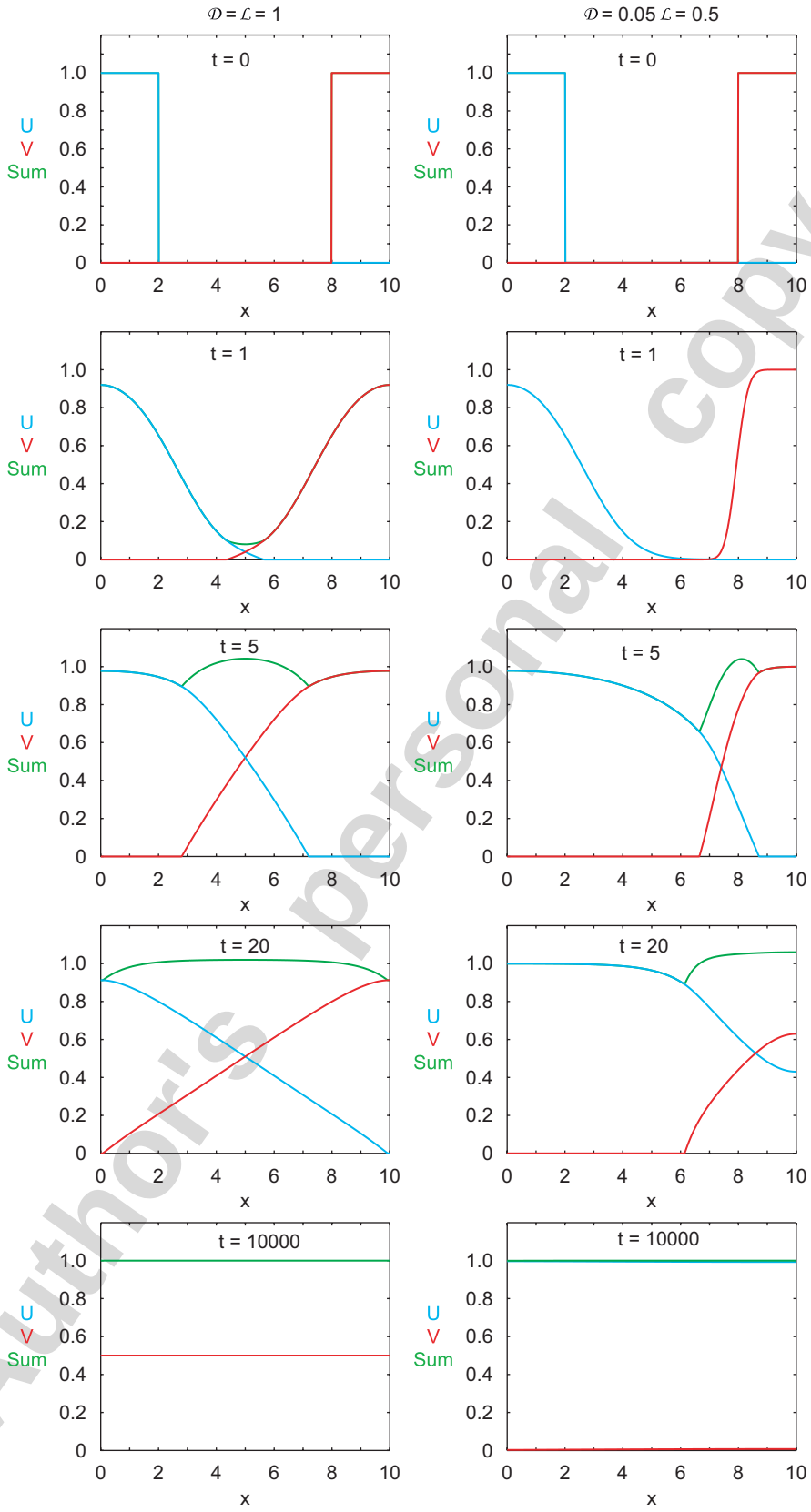

Fig. 13. Temporal evolution of coalescence with diffusivity functions specified by Sherratt (2000), $f(u,v) = u/(u+v)$, $g(u,v) = v/(u+v)$. Results are shown for $\mathcal{D} = \mathcal{L} = 1$ in the left-hand column at $t = 0, 1, 5, 20$ and $t = 10\,000$. Details of the $u(x,t)$ (blue), $v(x,t)$ (red) and the sum $u(x,t) + v(x,t)$ (green) are shown. Equivalent results are shown in the right-hand column for $\mathcal{D} = 0.05$ and $\mathcal{L} = 0.5$. Numerical simulations are evaluated with $\Delta x = 0.01$ and variable Δt.

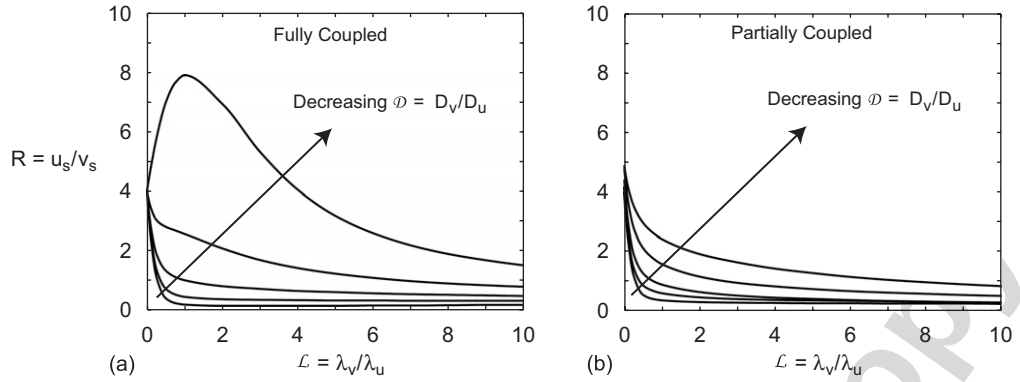

Fig. 14. Values of $R = u_s/v_s$ versus $\mathscr{L}$ for Sherratt's diffusivity functions with the initial condition (13) showing (a) fully coupled conditions and (b) partially coupled conditions. Five contours are shown for $\mathscr{D} = 0.25, 0.5, 1.0, 2.0$ and 5.0.

in assessing the validity of common assumptions underpinning many chimeric experimental systems. Chimeric assays are commonly used to distinguish between different cell types, such as the use of chick-quail grafting methods (Burns et al., 2002; Erickson, 1985; Le Douarin and Teillet, 1973; Le Douarin, 1973; Simpson et al., 2007). The critical underlying assumption in these experiments is that the donor and host cell types behave indistinguishably. Hence, these experiments assume that the donor and host cells have the same motility. This assumption, which is always implicit and untested, could be validated or challenged by making observations of the presence or absence of cell death in a coalescence assay.

The approach taken in this work provides two levels of detail regarding the simulation and interpretation of coalescence processes. Firstly, full details are obtained with the numerical simulations. This approach allows the steady-state solution to be exactly characterised in terms of the ratio R. Secondly, and more generally, we analytically determine conditions guaranteeing that the transient solution never becomes overcrowded for all $t>0$. While the exact steady-state R depends on the initial condition and domain geometry, this is not true of the conditions regarding the absence of overcrowding. For any initial condition satisfying $0 \leqslant u(x,0) + v(x,0) \leqslant 1$ on any $0 < x < L$ the solution never becomes overcrowded for all $t>0$ provided that both cell populations have identical diffusivities. This is a very strong, general result. This suggests that an existing cell migration assay (Fig. 2) can be used in a new way to determine whether two different cell populations are governed by the same motility mechanism.

A final and important point can be made regarding the question of whether the logistic-type source terms are appropriate to represent overcrowding and cell death. A common assumption in continuum models of cell invasion phenomena is that cells proliferate to a carrying capacity limit, and that a logistic (Murray, 2002) or similar source term (Tsoularis and Wallace, 2002) governs this process. In virtually all theoretical applications, the source term is positive and acts to increase the cell density as the invasion process proceeds. However, the current study and other recent theoretical work (Simpson et al., 2006b) have investigated interactions of invasive cell populations where the logistic source terms act as a sink due to overcrowding. We suggest that a thorough examination of experimental systems involving the interaction of invasive cell populations will be of enormous interest to the theoretical biology community as it is unclear whether or not logistic-type terms are appropriate to represent overcrowding and cell death processes.

Acknowledgements

This work is supported by the National Health and Medical Research Council and the Australian Research Council (ARC). Mat Simpson is an ARC Postdoctoral Fellow. Kerry Landman is supported by the Particulate Fluids Processing Centre, an ARC Special Research Centre. We thank Don Newgreen, Heather Young, Barry Hughes, Tom Witelski and Phil Broadbridge for many helpful discussions. The comments from the three anonymous reviewers are appreciated.

Appendix A. Numerical algorithm

Eqs. (3)–(4) will be integrated from t^k to t^{k+1} with $\Delta t^k = t^{k+1} - t^k$. Variable time steps will be used and Δt will be referred to without the superscript unless necessary. Spatial derivatives are replaced with standard centred in space finite difference approximations on a uniformly spaced grid with N nodes. The semi-discrete odes at the ith internal node are given by

$$\frac{\mathrm{d}u_i}{\mathrm{d}t} = \frac{1}{\Delta x^2}\left(f_{i+1/2}[u_{i+1} - u_i] - f_{i-1/2}[u_i - u_{i-1}]\right) + u_i(1 - v_i - u_i), \tag{22}$$

$$\frac{\mathrm{d}v_i}{\mathrm{d}t} = \frac{\mathscr{D}}{\Delta x^2}\left(g_{i+1/2}[v_{i+1} - v_i] - g_{i-1/2}[v_i - v_{i-1}]\right) + \mathscr{L} v_i(1 - v_i - u_i). \tag{23}$$

With starting values u_i^k and v_i^k, trial values of u_i^{k+1} and v_i^{k+1} are evaluated with a backward Euler time step. The discrete equations are linearised with a standard Picard linearisation with iteration index m. The linearised equations can be written as

$$\frac{u_i^{k+1,m+1}-u_i^k}{\Delta t}=\frac{1}{\Delta x^2}\left(f_{i+1/2}^{k+1,m}\left[u_{i+1}^{k+1,m+1}-u_i^{k+1,m+1}\right]-f_{i-1/2}^{k+1,m}\left[u_i^{k+1,m+1}-u_{i-1}^{k+1,m+1}\right]\right)+u_i^{k+1,m+1}(1-v_i^{k+1,m}-u_i^{k+1,m}), \quad (24)$$

$$\frac{v_i^{k+1,m+1}-v_i^k}{\Delta t}=\frac{\mathscr{D}}{\Delta x^2}\left(g_{i+1/2}^{k+1,m}\left[v_{i+1}^{k+1,m+1}-v_i^{k+1,m+1}\right]-g_{i-1/2}^{k+1,m}\left[v_i^{k+1,m+1}-v_{i-1}^{k+1,m+1}\right]\right)+\mathscr{L}v_i^{k+1,m+1}(1-v_i^{k+1,m}-u_i^{k+1,m+1}). \quad (25)$$

The internode diffusivities are evaluated with an arithmetic average. The linear systems for u and v are solved sequentially to take advantage of the tridiagonal matrix structure and the Thomas algorithm. Picard iterations are conducted until an absolute convergence test is satisfied

$$\max|c_i^{k+1,m+1}-c_i^{k+1,m}|<\tau_P \quad \text{for} \quad i=1,2,3,\ldots,N, \quad (26)$$

where c_i represents either u_i or v_i. The temporal derivative across the time step is approximated by

$$\left(\frac{\mathrm{d}c}{\mathrm{d}t}\right)_i^{k+1}=\frac{c_i^{k+1}-c_i^k}{\Delta t} \quad \text{for} \quad i=1,2,3,\ldots,N. \quad (27)$$

A measure of the local truncation error associated with the backward Euler approximation is given by

$$e_i^{k+1}=\frac{\Delta t}{2}\left|\left(\frac{\mathrm{d}c}{\mathrm{d}t}\right)_i^{k+1}-\left(\frac{\mathrm{d}c}{\mathrm{d}t}\right)_i^{k}\right| \quad \text{for} \quad i=1,2,3,\ldots,N. \quad (28)$$

To implement (28), values of $(\mathrm{d}c/\mathrm{d}t)_i^k$ are retained from the previous time step. For the very first step values of $(\mathrm{d}c/\mathrm{d}t)_i^0$ are calculated from the initial conditions. The current step is accepted provided that an absolute convergence test is satisfied

$$\max(\mathrm{e}_i^{k+1,m+1})=\mathrm{e}^{k+1,m+1}<\tau_T \quad \text{for} \quad i=1,2,3,\ldots,N. \quad (29)$$

If this error test is not satisfied, then Δt is reduced and the temporal integration is re-attempted with a smaller Δt. The reduced time step is given by

$$\Delta t_{\text{reduced}}=\Delta t_{\text{failed}}\times\max\left(s\sqrt{\frac{\tau_T}{\max(\mathrm{e}^{k+1,m+1},\varepsilon)}},r_{\min}\right). \quad (30)$$

The maximum time step reduction rate is set to $r_{\min}=0.5$. The safety factor is $s=0.9$ (Sloan and Abbo, 1999) and the machine precision $\varepsilon=1\times10^{-10}$ prevents floating point errors.

If the error test is satisfied, the backward Euler approximations are locally extrapolated to second-order accuracy,

$$c_i^{k+1}=c_i^k+\frac{\Delta t}{2}\left[\left(\frac{\mathrm{d}c}{\mathrm{d}t}\right)_i^{k}+\left(\frac{\mathrm{d}c}{\mathrm{d}t}\right)_i^{k+1}\right] \quad \text{for} \quad i=1,2,3,\ldots,N. \quad (31)$$

These estimates are stored as the solution and the algorithm attempts a new time step. At the beginning of each new time step a forward Euler expression is used to approximate starting values of $u^{k+1,0}$ and $v^{k+1,0}$. Compared to the usual approach of setting $u^{k+1,0}=u^k$ and $v^{k+1,0}=v^k$, we have found that the linearisation iterations converge faster with the forward Euler estimates. These estimates are given by

$$c_i^{k+1,0}=c_i^k+\Delta t\left(\frac{\mathrm{d}c}{\mathrm{d}t}\right)_i^{k} \quad \text{for} \quad i=1,2,3,\ldots,N. \quad (32)$$

Each new time step is attempted with an enlarged Δt,

$$\Delta t_{\text{enlarged}}=\Delta t_{\text{accepted}}\times\min\left(s\sqrt{\frac{\tau_T}{\max(\mathrm{e}^{k+1,m+1},\varepsilon)}},r_{\max}\right). \quad (33)$$

Here $r_{\max}=2.0$ to ensure that the step size changes are not too abrupt.

To stop the algorithm we implement one of two approaches depending on the purpose of the simulation. Firstly, if the algorithm is to be executed until a particular time t_{stop}, we test at the beginning of each time step to see whether the next step will advance the solution past this point. Once the algorithm establishes that the next step will advance the system beyond t_{stop}, the time step is reduced so that the time step takes the solution exactly to t_{stop}. Secondly, if the algorithm is used to solve for the long-time steady solution, we test to see when the solutions are spatially invariant. This involves evaluating both the maximum and minimum values of u and v. The solution is deemed to be steady when

$$\max(u_{\max}-u_{\min},v_{\max}-v_{\min})<\tau_S. \quad (34)$$

Once the algorithm reaches a time when (34) is satisfied, then it is deemed that the solution is steady and the algorithm stops.

All results presented in this work are obtained using $\tau_P=1\times10^{-5}$, $\tau_T=1\times10^{-4}$ and $\tau_S=1\times10^{-4}$. We found that further reducing these tolerances gave identical results and so this level of computing tolerance was adequate. All simulations were initiated with a very small time step $\Delta t^0=1\times10^{-5}$.

Appendix B. Linear stability analysis

To assess the stability of the steady-state solution satisfying $u_s+v_s=1$, we consider a small perturbation about the steady state given by

$$u=u_s+\varepsilon_1\mathrm{e}^{(\sigma t+\mathrm{i}kx)}, \quad v=v_s+\varepsilon_2\mathrm{e}^{(\sigma t+\mathrm{i}kx)}, \quad (35)$$

where $0<\varepsilon_1 \ll 1$, $0<\varepsilon_2 \ll 1$, k is the wave number and σ is the coefficient determining the stability about the steady state. The perturbations (35) are substituted into (3)–(4), assuming the first-order partial derivatives of $f(u,v)$ and $g(u,v)$ are bounded, the linear terms are retained giving the linearised system about the steady state. The eigenvalues are given by the determinant of the coefficient matrix of this linear system

$$\det\begin{bmatrix} \sigma + u_s + f(u_s,v_s)k^2, & u_s \\ \mathscr{L}v_s, & \sigma + \mathscr{L}v_s + \mathscr{D}g(u_s,v_s)k^2 \end{bmatrix} = 0. \tag{36}$$

The eigenvalues are given by $\sigma_\pm = (-\mathscr{M} \pm \sqrt{\mathscr{M}^2 - 4\mathscr{N}})/2$ with

$$\mathscr{M} = u_s + \mathscr{L}v_s + k^2[\mathscr{D}g(u_s,v_s) + f(u_s,v_s)], \tag{37}$$

$$\mathscr{N} = k^2[\mathscr{D}u_s g(u_s,v_s) + \mathscr{L}v_s f(u_s,v_s)] + \mathscr{D}f(u_s,v_s)g(u_s,v_s)k^4. \tag{38}$$

For stability we require both $\Re(\sigma_\pm)<0$, which in turn requires both $\mathscr{M}>0$ and $\mathscr{N}>0$. These two conditions are always satisfied according to (37)–(38) as the constants u_s, v_s, $\mathscr{D}$, $\mathscr{L}$ and the functions $f(u_s,v_s)$ and $g(u_s,v_s)$ are positive by definition. Therefore, the steady-state solution $u_s + v_s = 1$ is stable for any $\mathscr{D}$, $\mathscr{L}$ and any $f(u,v)$ and $g(u,v)$ whose first-order partial derivatives are bounded.

References

Allan, I.J., Newgreen, D.F., 1980. The origin and differentiation of enteric neurons of the intestine of the fowl embryo. Am. J. Anat. 157, 137–154.

Burns, A.J., 2005. Migration of neural crest-derived enteric nervous system precursor cells to and within the gastro intestinal tract. Int. J. Dev. Biol. 49, 143–150.

Burns, A.J., Delalande, J.-M.M., Le Douarin, N.M., 2002. In ovo transplantation of enteric nervous system precursors from vagal to sacral neural crest results in extensive hindgut colonization. Development 129, 2785–2796.

Cai, A., Landman, K.A., Hughes, B.D., 2006. Modeling directional guidance and motility regulation in cell migration. Bull. Math. Biol. 68, 25–52.

Cavazzoni, R., 2000. Diffusive approximation of Fisher's equation. Comput. Math. Appl. 39, 101–114.

Cohen, D.S., White, A.B.Jr., Witelski, T.P., 1995. Shock formation in a multi-dimensional viscoelastic diffusive system. SIAM J. Appl. Math. 55 (2), 348–368.

Denman, P.K., McElwain, D.L.S., Norbury, J., 2007. Analysis of travelling waves associated with the modelling of aerosolised skin grafts. Available online, Bull. Math. Biol. 69 (2), 495–523.

Dunbar, S.R., 1984. Travelling wave solutions of diffusive Lotka–Volterra equations: a heteroclinic connection in R^4. Trans. Am. Math. Soc. 268, 557–594.

Erickson, C.A., 1985. Control of neural crest cell dispersion in the trunk of the avian embryo. Dev. Biol. 111, 138–157.

Fisher, R.A., 1937. The wave of advance of advantageous genes. Ann. Eugenics 7, 353–369.

Gianino, S., Grider, J.R., Cresswell, J., Enomoto, H., Heuckeroth, R.O., 2003. GDNF availability determines enteric neuron number by controlling precursor proliferation. Development 130, 2187–2198.

Hearn, C.J., Murphy, M., Newgreen, D.F., 1998. GDNF and ET-3 differentially modulate the numbers of avian enteric neural crest cells and enteric neurons in vitro. Dev. Biol. 197, 93–105.

Hillen, T., Painter, K., 2001. Global existence for a parabolic chemotaxis model with prevention of overcrowding. Adv. Appl. Math. 26, 280–301.

Kavetski, D., Binning, P., Sloan, S.W., 2002. Adaptive backward Euler time stepping with truncation error control for numerical modelling of unsaturated fluid flow. Int. J. Numer. Meth. Eng. 53, 1301–1322.

Keller, E.F., Segel, L.A., 1970. Model for chemotaxis. J. Theor. Biol. 30, 225–234.

Landman, K.A., Pettet, G.J., Newgreen, D.F., 2003. Mathematical models of cell colonization of uniformly growing domains. Bull. Math. Biol. 65, 235–262.

Landman, K.A., Simpson, M.J., Slater, J.L., Newgreen, D.F., 2005. Diffusive and chemotactic cellular migration: smooth and discontinuous travelling wave solutions. SIAM J. Appl. Math. 65, 1420–1442.

Le Douarin, N., 1973. A biological cell labeling technique and its use in experimental embryology. Dev. Biol. 30, 217–222.

Le Douarin, N.M., Teillet, M.A., 1973. The migration of neural crest cells to the wall of the digestive tract in avian embryo. J. Embryol. Exp. Morphol. 30, 31–48.

Longo, D., Peirce, S.M., Skalak, T.C., Davidson, L., Marsden, M., Dzamba, B., DeSimone, D.W., 2004. Multicellular computer simulation of morphogenisis: blastocoel roof thinning and matrix assembly in *Xenopus laevis*. Dev. Biol. 271, 210–222.

Maini, P.K., McElwain, D.L.S., Leavesley, D., 2004a. Travelling waves in a wound healing assay. Appl. Math. Lett. 17, 575–580.

Maini, P.K., McElwain, D.L.S., Leavesley, D.I., 2004b. Traveling wave model to interpret a wound-healing cell migration assay for human peritoneal mesothelial cells. Tissue Eng. 10, 475–482.

McOwen, R.C., 1996. Partial Differential Equations, third ed. Prentice-Hall, Englewood Cliffs, NJ.

Merks, R.M.H., Glazier, J.A., 2005. A cell-centered approach to developmental biology. Physica A 352, 113–130.

Méndez, V., Ortega-Cejas, V., Campos, D., 2006. Front propagation in population dynamics with dispersive variability and delayed growth. Physica A 367, 283–292.

Murray, J.D., 2002. Mathematical Biology I: An Introduction, third ed. Springer, Heidelberg.

Murray, J.D., 2003. Mathematical Biology II: Spatial Models and Biomedical Applications, third ed. Springer, Heidelberg.

Painter, K.J., Sherratt, J.A., 2003. Modelling the movement of interacting cell populations. J. Theor. Biol. 225, 327–339.

Pao, C.V., 1992. Nonlinear Parabolic and Elliptic Equations. 3rd ed. Plenum Press, New York.

Peirce, S.M., VanGieson, E.J., Skalak, T.C., 2004. Multicellular simulation predicts microvascular patterning and in silico tissue assembly. FASEB J., 10.1096/fj.03-0933fje.

Perumpanani, A.J., Sherratt, J.A., Norbury, J., 1997. Mathematical modeling of capsule formation and multinodularity in benign tumour growth. Nonlinearity 10, 1599–1614.

Protter, M.H., Weinberger, H.F., 1967. Maximum Principles in Differential Equations. Prentice-Hall, Englewood Cliffs, NJ.

Savla, U., Olson, L.E., Waters, C.M., 2004. Mathematical modeling of airway epithelial wound closure during cyclic mechanical strain. J. Appl. Physiol. 96, 566–574.

Sherratt, J.A., 2000. Wavefront propagation in a competition equation with a new motility term modelling contact inhibition between cell populations. Proc. R. Soc. London A. 456, 2365–2386.

Shigesada, N., 1980. Spatial distribution of dispersing animals. J. Math. Biol. 9, 85–96.

Simpson, M.J., Clement, T.P., 2003. Theoretical analysis of the worthiness of Henry and Elder problems as benchmarks of density-dependent groundwater flow models. Adv. Water Resour. 26, 17–31.

Simpson, M.J., Clement, T.P., 2004. Improving the worthiness of the Henry problem as a benchmark for density-dependent groundwater flow models. Water Resour Res. 40, W01504.

Simpson, M.J., Landman, K.A., Newgreen, D.F., 2006a. Chemotactic and diffusive migration on a nonuniformly growing domain: numerical algorithm development and applications. J. Comput. Appl. Math. 192, 282–300.

Simpson, M.J., Landman, K.A., Hughes, B.D., Newgreen, D.F., 2006b. Looking inside an invasion wave of cells using continuum models: proliferation is the key. J. Theor. Biol. 243, 343–360.

Simpson, M.J., Zhang, D.C., Mariani, M., Landman, K.A., Newgreen, D.F., 2007. Cell proliferation drives neural crest cell invasion of the intestine. Dev. Biol. 302, 553–568.

Sloan, S.W., Abbo, A.J., 1999. Biot consolidation analysis with automatic time stepping and error control Part 1: theory and application. Int. J. Numer. Anal. Meth. Geomech. 23, 467–492.

Tsoularis, A., Wallace, J., 2002. Analysis of logistic growth models. Math. Biosci. 179, 21–55.

Tyson, R., Lubkin, S.R., Murray, J.D., 1999. A minimal mechanism for bacterial pattern formation. Proc. R. Soc. London B. 266, 299–304.

Witelski, T.P., 1995. Merging traveling waves for the porous-Fisher's equation. Appl. Math. Lett. 8, 27–32.

Witelski, T.P., 1997. Segregation and mixing in degenerate diffusion in population dynamics. J. Math. Biol. 35, 695–712.

Wolpert, L., 2002. Principles of Development. Oxford University Press, Oxford, UK.

Young, H.M., Hearn, C.J., Farlie, P.G., Canty, A.J., Thomas, P.Q., Newgreen, D.F., 2001. GDNF is a chemoattractant for enteric neural cells. Dev. Biol. 229, 503–516.

Young, H.M., Bergner, A.J., Anderson, R.B., Enomoto, H., Milbrandt, J., Newgreen, D.F., Whitington, P.M., 2004. Dynamics of the neural crest-derived cell migration in the embryonic mouse gut. Dev. Biol. 270, 455–473.